

CHAPTER 3
TROPOSPHERIC CLEAR-AIR EFFECTS

3.1 INDEX OF REFRACTION PROFILE

Propagation in the troposphere is influenced, and in some cases strongly affected, by the variation of the index of refraction with height. By definition, the index of refraction n of a particular type of wave in a given medium is the ratio of c , about 2.9979×10^8 m/s, to the phase velocity of the wave in the medium. The index of refraction of the troposphere is a function of pressure, temperature, and water vapor content as indicated by

$$N = (n - 1) \times 10^6 = \frac{77.6 p_d}{T} + \frac{72 e}{T} + \frac{3 \times 10^5 e}{T^2} \quad (3.1)$$

where p_d is the pressure of dry nonpolar air in mb (millibars), e is water vapor pressure in mb, and T is temperature in kelvins (Smith and Weintraub, 1953). Because the index n is only slightly greater than 1, the usual practice is to use N units for convenience, with N defined as in Eq. (3.1). N , referred to as refractivity, is seen to vary inversely with temperature and to be strongly dependent on water vapor pressure. The water vapor pressure e , the saturation water vapor pressure e_s , which is a function of temperature (Table 3.1), and relative humidity R.H. are related by $e = e_s$ (R.H.). If Eq. (3.1) is expressed in terms of p , the total pressure, where $p = p_d + e$, it becomes

$$N = \frac{77.6 p}{T} - \frac{5.6 e}{T} + \frac{3.75 \times 10^5 e}{T^2} \quad (3.2)$$

The last two terms can be combined to give, approximately,

$$N = \frac{77.6 p}{T} + \frac{3.73 \times 10^5 e}{T^2} = \frac{77.6}{T} \left[p + \frac{4810 e}{T} \right] \quad (3.3)$$

The two forms of Eq. (3.3) are widely used (CCIR, 1986a) and give

values for N that are accurate within 0.5 percent for the ranges of atmospheric parameters normally encountered and for frequencies below 30 GHz (Crone, 1976). If one wishes to consider the effects of dry air and water vapor separately, however, letting $N = N_d + N_w$ where N_d refers to dry air and N_w to water vapor, Eq. (3.1) should be used with

$$\epsilon_d = 77.6 \text{ pal/T} \quad (3.4)$$

and

$$N_w = \frac{72 e}{T} + \frac{3.75 \times 10^5 e}{T^2} \quad (3.5)$$

Table 3.1 Saturation Water Vapor Pressure e_s from List (1984) in Smithsonian Meteorological Tables.]

T (°C)	e_s (rob)	T (°C)	e_s (rob)
-30	0.5	18	20.6
-20	1.3	20	23.4
-10	2.9	22	26.4
0	6.1	24	29.8
2	7.1	26	33.6
4	8.1	28	37.8
6	9.3	30	42.4
8	10.7	32	47.6
10	12.3	34	53.2
12	14.0	36	59.4
14	16.0	38	66.3
16	18.2	40	73.8

The absolute humidity or water vapor density in g/m^3 , ρ , and e in mb are related (Appendix 3.1) by

$$\rho = 216.5 \frac{e}{T} \quad (3.6)$$

The dew point is the temperature at which air is saturated with water vapor, and values of the dew point can be used to determine the saturation water vapor pressure by use of Table 3.1. For example, the highest accepted weather-observatory dew point of 34 deg C [recorded on the shore of the Persian Gulf at Sharjah, Saudi Arabia (U.S. Standard Atmosphere, 1976)] corresponds to a vapor pressure of 53.2 mb and an absolute humidity of 37.5 grams per cubic meter. Although an increase in temperature would cause a decrease in N if water vapor pressure were held constant, the saturation pressure increases rapidly with temperature and the highest values of N therefore occur for high temperatures (and high relative humidities).

The value of N corresponding to the value of e of 53.2 mb at a temperature of 34 deg C, for example, is 467. In nearby desert areas of Saudi Arabia where the relative humidity might approach zero, however, the value of N could approach 256, the value for dry air at the sea level pressure of 1013 mb and the temperature of 34 deg C. The lowest surface values of N tend to occur in high, dry areas where both ρ and e are low. At a height of 3 km, for example, assuming the pressure for a standard atmosphere but a temperature of 273 K, N is 230 with 100 percent relative humidity and 199 with 0 percent humidity. The values of N mentioned above are extreme. Monthly mean values of N at sea level vary between about 290 and 400 within ± 25 deg of latitude from the equator, with a somewhat smaller variation elsewhere, and are typically 320 in winter and 340 in summer in the UK (Hall, 1979). In the United States, winter values vary from about 285 to 345 and summer values range from about 275 to 385 (Bean and Dutton, 1966).

Pressure, temperature, and water vapor content all decrease with height above the Earth's surface in the troposphere on the average, but temperature increases with height in temperature inversion layers. Pressure drops off approximately exponentially with height, and the decrease or change of e with height is variable

but may be approximately exponential. The refractivity N may also decrease with height in a variable manner but on the average tends to decrease exponentially as described by

$$N = N_s e^{-h/H} \quad (3.7)$$

where N is the refractivity at the height h above the level where the refractivity is N_s . H is the applicable scale height. The change in N in the first km of height above the surface, ΔN , is a parameter of significance. In the average atmosphere as defined by the CCIR, N_s has the value of 315 and ΔN the value of -40 consistent with

$$N = 315 e^{-0.136 h} \quad (3.8)$$

with h in km (CCIR, 1986a). Values of N_s and ΔN have been compiled, with N_s sometimes reduced to sea level values. Charts showing these quantities, probability distributions of N_s , water vapor density p , etc. have been provided by Bean, Horn, and Ozanich (1960), Bean et al. (1966), and the CCIR (1986a). Figure 3.1 shows annual cycles of N_s for several climatic types.

The exponential model is widely applicable but any reliable data on actual refractivity profiles should be used when available. Such data can be acquired by use of radiosondes or microwave refractometers and often display significant departure from the exponential form. A common cause of non-exponential refractivity profiles is the occurrence of temperature-inversion layers. In an inversion layer, the temperature increases with altitude. Such a layer is highly stable (Sec. 1.3). All vertical motions are strongly inhibited in an inversion layer, and pollution and water vapor existing below the layer tend to be confined below it. Temperature inversions may develop when the loss of heat from the surface of the Earth is not compensated by inputs of heat, the ground being a more efficient radiator than air and therefore cooling more rapidly. Surface and low-level inversions tend to develop at night and in the arctic and subarctic in winter and in locations such as the San Joaquin Valley of California where fog forms under the inversion and prevents surface heating in winter. Inversions may form also when warm air blows over a cool ocean.

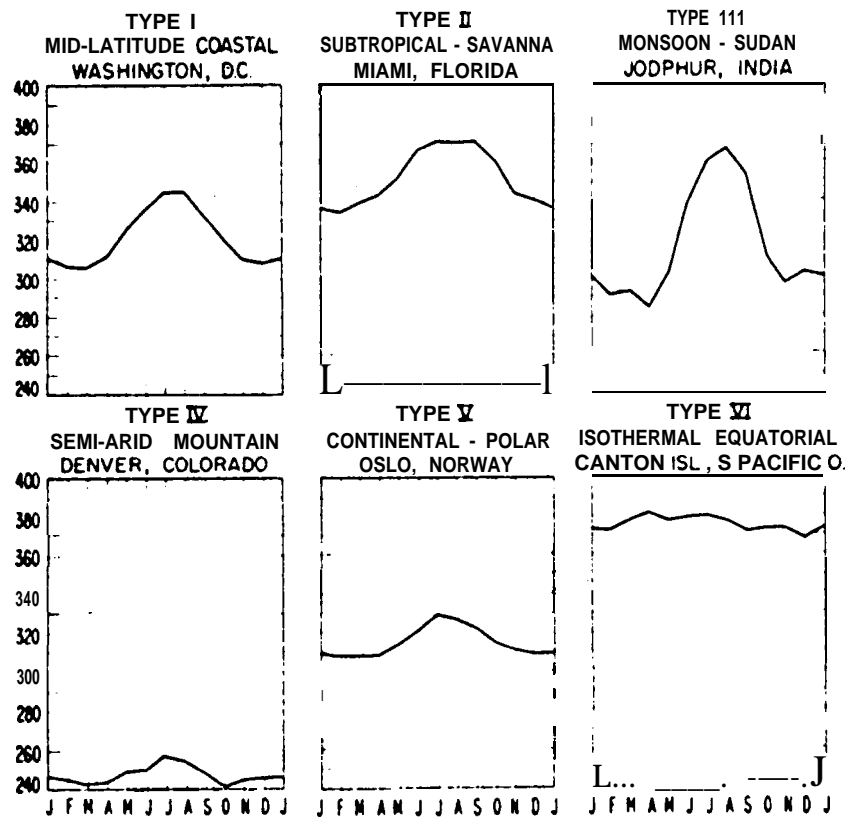


Figure 3.1. Annual cycles of Ns by climatic type (Bean, Horn, and Ozanich, 1950).

Inversions are also caused by subsiding air, and this type of inversion is common because in portions of developing or semipermanent anticyclones the air between about 500 and 5000 m descends at a rate typically about 1000 m/day (Scorer, 1968). The Pacific coast of the United States lies along the eastern edge of a semipermanent anticyclone that forms in the Pacific, and the persistent temperature inversion of the Los Angeles area is caused largely by subsiding air. This air is heated in a process of adiabatic compression but the movement and heating cannot extend to the ground itself, and a temperature inversion is formed at or near the surface.

The occurrence of a high water vapor content underneath an inversion layer may be accompanied by a rapid decrease in water vapor content through the inversion layer. The corresponding N value is also high beneath the layer and drops abruptly through the layer in such a case.

3.2 REFRACTION AND FADING

A practical consequence of the variation of the index of refraction of the troposphere with height is that electromagnetic waves do not travel in straight lines but experience refraction or bending. To treat this phenomenon, consider ray paths which represent paths along which energy is transmitted. An important characteristic of an element of a ray path is its curvature C, defined as $1/\rho$ where ρ is the radius of curvature. It can be shown (Bean and Dutton, 1966; Flock, 1979) that a ray path in a spherically stratified atmosphere has a curvature given by

$$C = - \frac{1}{n} \frac{dn}{dh} \cos \beta \quad m^{-1} \quad (3.9)$$

where β is the angle of the ray measured from the horizontal. In the troposphere $n \approx 1$, and for rays having an angle β that is near zero, the expression for C simplifies to

$$C = - dn/dh \quad (3.10)$$

This latter form is used for terrestrial line-of sight paths.

The change in direction, or the amount of bending, τ , along a path can be determined by taking $\tau = \int C ds$ or $\tau = \sum C \Delta s$ where ds is an infinitesimal element of length and Δs is a finite element of length. In a length ds the corresponding bending $d\tau$ is given by

$$d\tau = - \frac{1}{n} \frac{dn}{dh} \cos \beta ds \quad \text{rad} \quad (3.11)$$

But as $dh = \sin \beta ds$

$$d\tau = - \frac{dn}{n \tan \beta} \quad (3.12)$$

This form can be used for ray tracing for any arbitrary index of refraction profile and for a path at any angle (Weisbrod and Anderson, 1959; Flock, 1979).

Very-low-angle satellite paths may experience much the same effects as terrestrial line-of-sight paths. To illustrate these effects we use the simple form $C = - dn/dh$ for propagation over a spherical earth. In this case the difference in curvature between a ray path and the Earth's surface is given by

$$\frac{1}{r_0} - C = \frac{1}{r_0} + \frac{dn}{dh} \quad (3.13)$$

where r_0 is the Earth's radius and $1/r_0$ is the corresponding curvature. To analyze propagation, one can use a geometric transformation such that ray paths become straight lines and the Earth has an effective radius k times the true radius r_0 . Thus

$$\frac{1}{r_0} + \frac{dn}{dh} = \frac{1}{kr_0} + 0 \quad (3.14)$$

which maintains the same relative curvature as in Eq. (3.13). The 0 has been included on the right-hand side of Eq. (3.14) to emphasize that it applies to the case that $dn/dh = 0$, for which case the ray paths are straight lines. In terms of N units the relation is

$$\frac{1}{kr_0} = [157 + dN/dh] \times 10^{-6} \quad (3.15)$$

The relation of Eq. (3. 15) is illustrated by Table 3.2.

Table 3.2 Corresponding Values of dN/dh and k .

dN/dh (N/km)	k
157	0.5
78	2/3
0	1.0
-40	4/3
-100	2.75
-157	∞
-200	-3.65
-300	-1.09

Typically, $dN/dh = -40$ and $k = 4/3$, and graphs prepared for $k = 4/3$ have been used for plotting terrestrial microwave paths. However, k can vary over a range of values, and this type of graphical procedure has the shortcoming that a different graph is needed for each k value.

A more efficient procedure is to use a transformation which makes the Earth flat and allows plotting paths for various k values on the same chart. Such plots are made by calculating h' of Fig. 3.2 in accordance with

$$h' = d_1 d_2 / (12.75 k) \quad \text{m} \quad (3.16)$$

where d_1 and d_2 are the distances from the two ends of the path (GTE, 1972). The units of Eq. (3.16) are km for d_1 and d_2 and m for h' . The basis for Eq. (3.16) is that $h' = h_{\max} - h$ where h_{\max} and h are calculated with respect to the center of the path by using, for h for example,

$$h = 1^2 / (12.75 k) \quad \text{m} \quad (3.17)$$

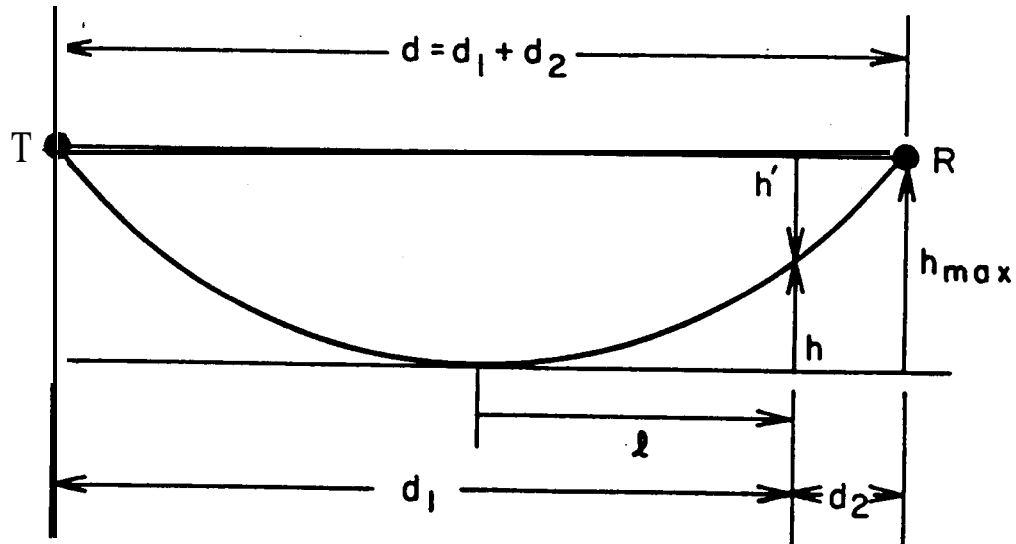


Figure 3.2. Quantities referred to for flat-earth plot.

where l is the horizontal distance from the center of the path, at which point the path is horizontal, to where h is specified. The distance l is in km and h is in m in Eq. (3.17). This expression follows from the construction of Fig. 3.3 where, in contrast to Fig. 3.2, the ray path is straight and the Earth is curved. Here l , r_0 , and $r_0 + h$ form the three sides of a right triangle. For $h \ll r_0$, it can be determined that

$$h = l^2/2r_0 \quad (3.18)$$

with all quantities in identical units. For a finite value of dn/dh , however, r_0 is replaced by kr_0 , and the form of Eq. (3.17) results when l is in km and h is in m.

The effect of the various k values is illustrated in exaggerated form in Figs. 3.4 and 3.5. In Fig. 3.4 all the rays are horizontal at the common point. In Fig. 3.5 ray paths are shown which allow signals from a common transmitter to reach a common receiving location.

It is evident from the above discussion that tropospheric refraction may cause errors in the measurement of elevation angle and variations in angle of arrival which can cause a reduction of

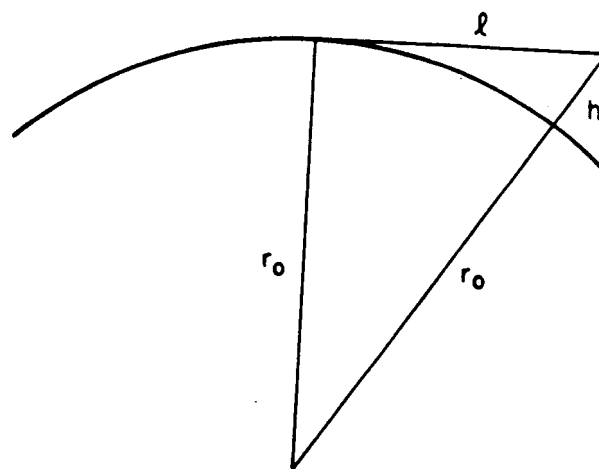


Figure 3.3. Geometry for determining h for initially horizontal rays.

signal amplitude for narrow-beam antennas. Also some degree of beam spreading or defocusing may occur and cause an attenuation of up to about 0.4 dB (Hall, 1999). To visualize how such defocusing occurs, consider a family of relatively closely spaced rays within an antenna beamwidth. The closer the spacing of the rays, the greater the signal intensity is. Defocusing involves a distortion of the ray paths such that the rays are more widely spaced than normally in the region of the receiving antennas.

Various programs for calculating bending have been devised. A simple procedure for calculating bending and elevation angle errors was presented by Weisbrod and Anderson (1959). Bending angles have been calculated by Crane (1976) for different elevation angles and for the 1966 U.S. Standard Atmosphere and an assumed humidity profile. His values are given in Table 3.3. The ray paths extend from the surface to the heights shown, and the heights correspond to the ranges or path lengths shown. The exact values of the bending angles vary depending on atmospheric conditions, but the values of Table 3.3 are representative. Also included are values of range error or excess range (Sec. 3.7). For transmitted or radar targets in the troposphere, the total bending and elevation angle errors are not the same; for astronomical sources and

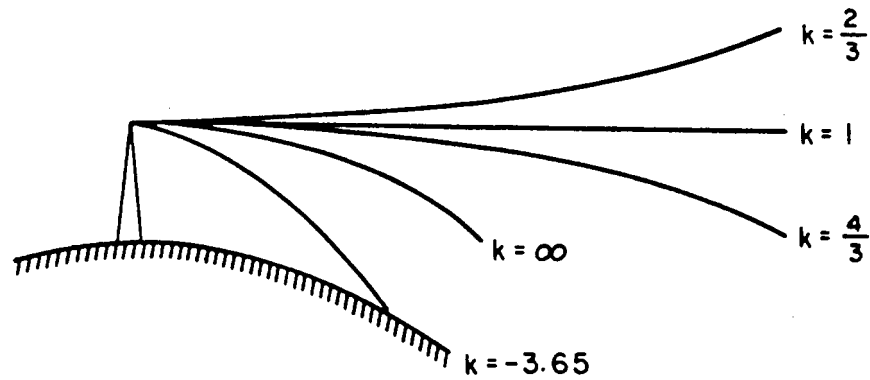


Figure 3.4. Ray paths for several values of k for initially horizontal rays (exaggerated and illustrative only).

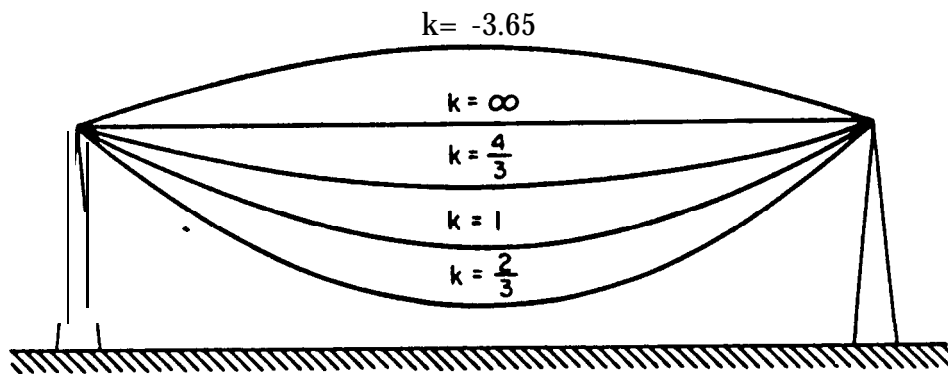


Figure 3.5. Ray paths from a transmitter T to a receiver R for various value of k (exaggerated and illustrative only).

geostationary satellites, the total bending and elevation error angles are identical. Bending takes place largely in the lower troposphere and Crane (1976) has shown that for a horizontally stratified atmosphere the total bending τ is related to surface refractivity N_s by $\tau = a + b N_s$, where the coefficients a and b vary with elevation angle and have been tabulated in his paper for Albany, New York. Nearly the same values are said to apply in other circumstances.

A phenomenon of major importance in tropospheric propagation at small angles from the horizontal, especially in the presence of temperature inversions, is the occurrence of severe fading due to multipath propagation. Propagation over more than one path may involve reflection from land and water surfaces and from manmade structures. This type of multipath is considered in Chap. 6. Multipath propagation involving the atmosphere alone, such as suggested in Fig. 3.6, however, also occurs. In terrestrial line-of-sight links, a fading allowance of 30 to 45 dB is commonly assigned for multipath fading. Such paths are often essentially horizontal or at only a slight angle from the horizontal, whereas earth-space paths are usually at rather large angle above the horizontal for which tropospheric fading is much less severe. It is often considered that about 5 to 10 deg is the smallest elevation angle that should be employed for earth-space paths, but there are circumstances for which it may be necessary to operate at lower angles, as at high latitudes. Then atmospheric multipath fading may prove to be as serious as for terrestrial paths.

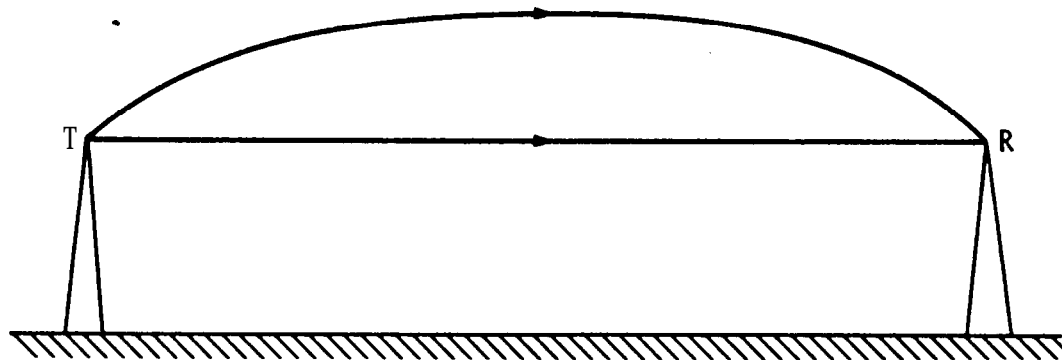


Figure 3.6. Atmospheric multipath propagation,

Table 3.3 Ray Parameters for a Standard Atmosphere^{a,b} for Rays from the Surface to Indicated Heights (Crane, 1976).

Initial Elev. Angle (deg)	Height (km)	Range (km)	Bending (mdeg)	Elev.-Angle Error (mdeg)	Range Error (m)
0.0	0.1	41.2	97.2	48.5	12.63
	1.0	131.1	297.9	152.8	38.79"
	5.0	289.3	551.2	310.1	74.17
	25.0	623.2	719.5	498.4	101.0
	80.0	1081.1	725.4	594.2	103.8
5.0	0.1	1.1	2.6	1.3	0.34
	1.0	11.4	25.1	12.9	3.28
	5.0	55.2	91.7	52.4	12.51
	25.0	241.1	176.7	126.3	24.41
	80.0	609.0	181.0	159.0	24.96
50.0	0.1	0.1	0.2	0.1	0.04
	1.0	" 1.3	1.9	1.0	0.38
	5.0	6.5	7.0	4.0	1.47
	25.0	32.6	14.3	10.3	3.05
	80.0	104.0	14.8	13.4	3.13

^aU.S. Standard Atmosphere Supplements, 1966, Environmental Sci. Serv. Administration, Dept. of Commerce, Washington, DC (1966).

^bSissenwine, N., D.D. Grantham, and H.A. Salmela, AFCRL-68-0556, Air Force Cambridge Res. Lab., Bedford, MA (Oct. 1968).

3.3 DUCTING

Ducting is a severe refractive effect involving trapping of a wave in a duct, commonly a surface duct, and possibly propagation for an abnormally long distance. Ducting occurs frequently in some locations, but it is not a reliable means of communication. It can, however, cause interference beyond the horizon, at a location that would otherwise be free from interfering signals (Sec. 8.5; Dougherty and Hart, 1976; Dougherty and Hart, 1979). A necessary condition for ducting to occur is that the refractivity decrease with height at a rate of 157 N units per km or greater. If $dN/dh = -157$ Eq. (3.15) shows that $1/k r_0 = 0$, corresponding to $k = \infty$ (Figs. 3.4 and 3.5). A ray that is launched horizontally under this condition remains horizontal at a constant height relative to a spherical surface. If the rate of decrease of N is greater than 157 N/km, a ray may be bent downward to the surface of the Earth as for $k = -3.5$ in Fig. 3.4. Such a path may result in what has been called blackout fading (Hauteville, et al., 1980).

In such a case no signal reaches the receiving location and the use of space or frequency diversity may not improve the situation. The rays bent downward to the Earth's surface may be reflected upwards, however, and then refracted down to Earth again, etc., giving rise to ducting as illustrated in Fig. 3.7. A second condition for ducting is that the refractivity gradient of -157 N/km or greater be maintained over a height range of a number of wavelengths.

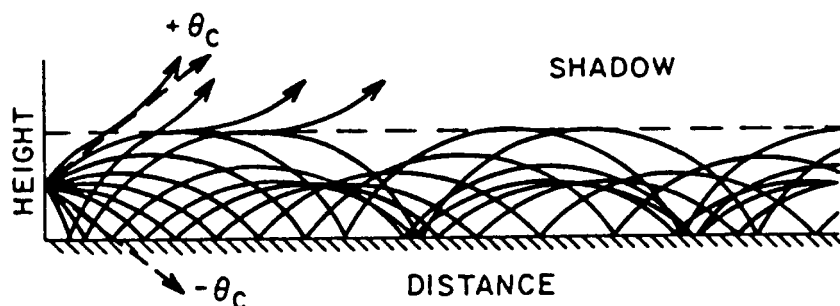


Figure 3.7. Example of ducting.

Ducting constitutes a mechanism for interference between earth stations and terrestrial line-of-sight systems and is considered further in Sec. 8.3.3. The free-space loss L_{FS} when expressed in dB as in Eq. (1.9) depends on distance as $20 \log d$, but for propagation in a duct the corresponding loss contribution is $10 \log d$. The reason is that in free space energy spreads out uniformly in all directions, but in a duct energy is constrained and spreads out in only two dimensions.

3.4 ATMOSPHERIC TURBULENCE

In addition to the variation of index of refraction with height, the index also exhibits variations associated with atmospheric turbulence. The theory of turbulence indicates that it develops from wind shear, that turbulence is introduced in the form of large turbulent eddies or blobs of scale size L_0 , and that energy is transferred from larger to smaller eddies throughout an inertial subrange corresponding to eddies of size l where $L_0 \geq l \geq l_0$. For eddies smaller than l_0 , viscous effects dominate and turbulent energy is dissipated. The process is suggested by Fig. 3.8. Associated with the turbulent eddies or blobs is a corresponding time-variable structure of temperature, water-vapor density, and index of refraction.

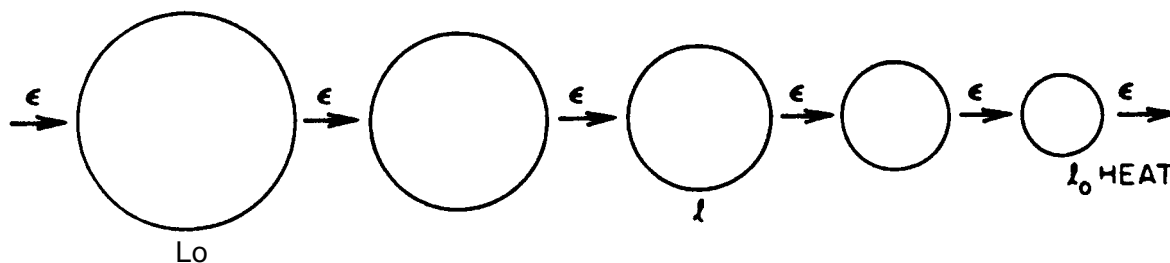


Figure 3.8. Illustration of the transfer of energy at the rate ϵ from large eddies to smaller eddies.

The quantity C_n^2 is a measure of the intensity of the index of refraction variations associated with turbulence. In particular.

$$C_n^2 = \overline{(n_1 - n_2)^2} \quad (3.19)$$

where n_1 and n_2 are values of the index of refraction at two locations a distance of 1m apart. The overbar indicates an average value of the quantity below it, namely $(n_1 - n_2)^2$. The atmosphere is normally turbulent to some degree, but the occurrence of turbulence is not uniform and a layered **structure** of turbulence tends to occur.

The turbulent structure of the index of refraction of the troposphere is believed to be largely **responsible** for the scatter of electromagnetic waves that is the basis for troposcatter communication systems and radar clear-air echoes. Scatter of this type is known as Bragg scatter and is due to the structure of the index of refraction that has a **periodicity** of λ' where

$$\lambda' = \lambda / [2 \sin (\theta/2)]$$

with λ the **electromagnetic wavelength** and θ the scattering angle as shown in Fig. 3.9. "The range of "eddy size is **large**, and scatter from turbulence can be expected to occur over a "wide range of frequencies and wavelengths.

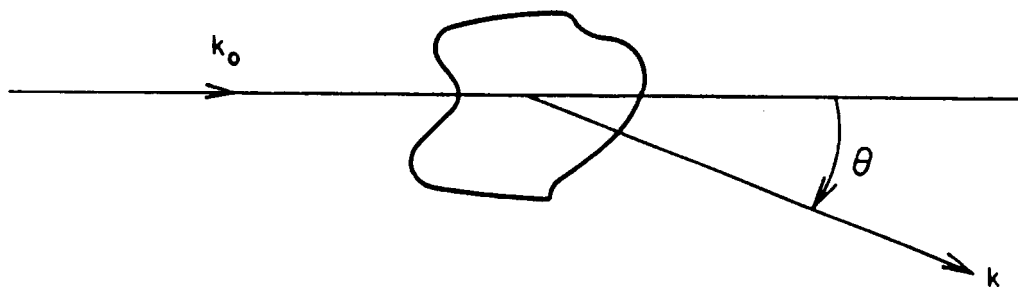


Figure 3.9. Scattering geometry.

For satellite communications, interest lies in the effect of turbulence on forward propagation through turbulent regions. The effects of forward propagation include amplitude fluctuations or scintillations, phase fluctuations, and angle-of-arrival variations.

3.5 AMPLITUDE VARIATIONS DUE TO REFRACTION AND TURBULENCE

It is not always easy to assess the relative importance of amplitude variations due to the large-scale profile of refractivity and due to small-scale structure associated with turbulence, either in advance planning or after the fact. Certain treatments of propagation emphasize one topic, and other studies deal with the other. In designing terrestrial line-of-sight links multipath fading associated with the refractivity profile receives attention, and effects of turbulence are largely ignored (GTE-Lenkurt, 1972). For earth-space paths the emphasis tends to be on effects due to turbulence (Theobald and Kaul, 1978).

The amplitude variations due to turbulence are smaller in general than those due to multipath propagation, as discussed in Sec. 3.2, tend to occur more rapidly or at higher frequencies, and are commonly referred to as scintillation. Such scintillation increases in amplitude with frequency (Thompson et al., 1975). For brevity we will henceforth refer to multipath fading for effects due to large-scale variations in refractivity and to scintillation for effects due to turbulence. Earth-space paths are at higher elevation angles than for terrestrial paths. Even paths at what are considered to be low angles for satellite communications tend to be at larger angles than those of terrestrial paths, for which severe multipath fading may occur. Also multipath fading, while severe at certain times of day and certain seasons in regions subject to strong temperature inversions, does not occur uniformly over large areas or uniformly with time. Earth-space paths tend to experience scintillation associated with turbulence more than multipath fading, especially at larger elevation angles and higher frequencies.

Low-angle satellite paths, however, can encounter both scintillation and multipath fading, and refractive multipath effects may dominate at low angles. On a path in Hawaii at an elevation

angle of 2.5 deg that simulated a low-angle earth-space at frequencies from 10 to 49 GHz, for example, Thompson et al. (1975) recorded both fades of more than 20 dB and scintillation of several dB in amplitude.

Measurements of 4 and 6 GHz signals at the very small elevation angle of one deg at Eureka in the Canadian arctic, some of which are summarized in Table 3.4, show effects that are probably due primarily to refractive multipath fading. Eureka is at a latitude of 80 deg on Ellesmere Island.

Table 3.4 6 GHz Margins for Tropospheric Fading at Eureka, Northwest Territories, Canada, Elevation Angle \approx 1 Degree (Strickland, et al., 1977).

Time Duration	Reliability		
	90%	99%	99.9%
Worst two hours	8.0 dB	18.0 dB	28.0 dB
Worst summer day	6.8 dB	15.5 dB	24.5 dB
Worst summer week (5 day)	5.4 dB	13.0 dB	22.0 dB
Worst month (July, i 5 days)	3.8 dB	10.8 dB	20.3 dB

Amplitude fluctuations and phase and angle-of-arrival variations due to turbulence are treated by Theobald and Kaul (1978), who include an example for a path at 28.56 GHz and an elevation angle of 10 deg. They predict a signal loss of 0.12 dB for clear weather, which is a small effect. Both the effects due to turbulence and the possibility of refractive fading would increase if the angle decreased below 10 deg. As noted earlier, Thompson et al. (1975) recorded larger scintillation of several dB at an angle of 2.5 deg in Hawaii.

3.6 GASEOUS ATTENUATION

A microwave absorption peak due to water vapor occurs at 22.235 GHz and peaks due to oxygen occur near 60 GHz and 118 GHz (CCIR, 1986b; Van Vleck, 1951; Waters, 1976; Liebe, 1985). Below 10 GHz absorption caused by atmospheric gases is small. Sea level values of the attenuation constant due to oxygen and water vapor are shown in Figure 3.10. Vertical one-way attenuation values from sea level for frequencies above 1 GHz are shown in Fig. 3.11. Attenuation values for paths at elevation angles θ above 10 deg are equal to the vertical values divided by $\sin \theta$, in a horizontally stratified atmosphere. The treatment by Smith (1982) of attenuation caused by atmospheric gases extends to frequencies below 10 GHz, and the thorough discussion by Liebe (1985) also includes examples for frequencies below 10 GHz.

Equation (3.20), based on the VanVleck-Weisskopf line shape, gives an expression for the sea level attenuation constant, or specific attenuation, in dB/km, due to oxygen for frequencies less than 57 GHz, with frequency f in GHz (CCIR, 1986b).

$$\alpha_0 = \left[0.00719 + \frac{6.09}{f^2 + 0.227} + \frac{4.81}{(f - 57)^2 + 1.50} \right] f^2 / 10^3 \quad \text{dB/km} \quad (3.20)$$

The attenuation caused by atmospheric gases plays a role in the determination of coordination distance for interference due to ducting and scatter from rain, and the same equation, but stated as applicable for frequencies less than 40 GHz, is given in Chap. 8 as Eq. (8.24). A complicated line structure appears between 57 and 63 GHz (CCIR, 1986 b). Such details can only be shown if an appropriate frequency scale is used. For water vapor, a corresponding expression, neglecting an absorption line near 320 GHz is

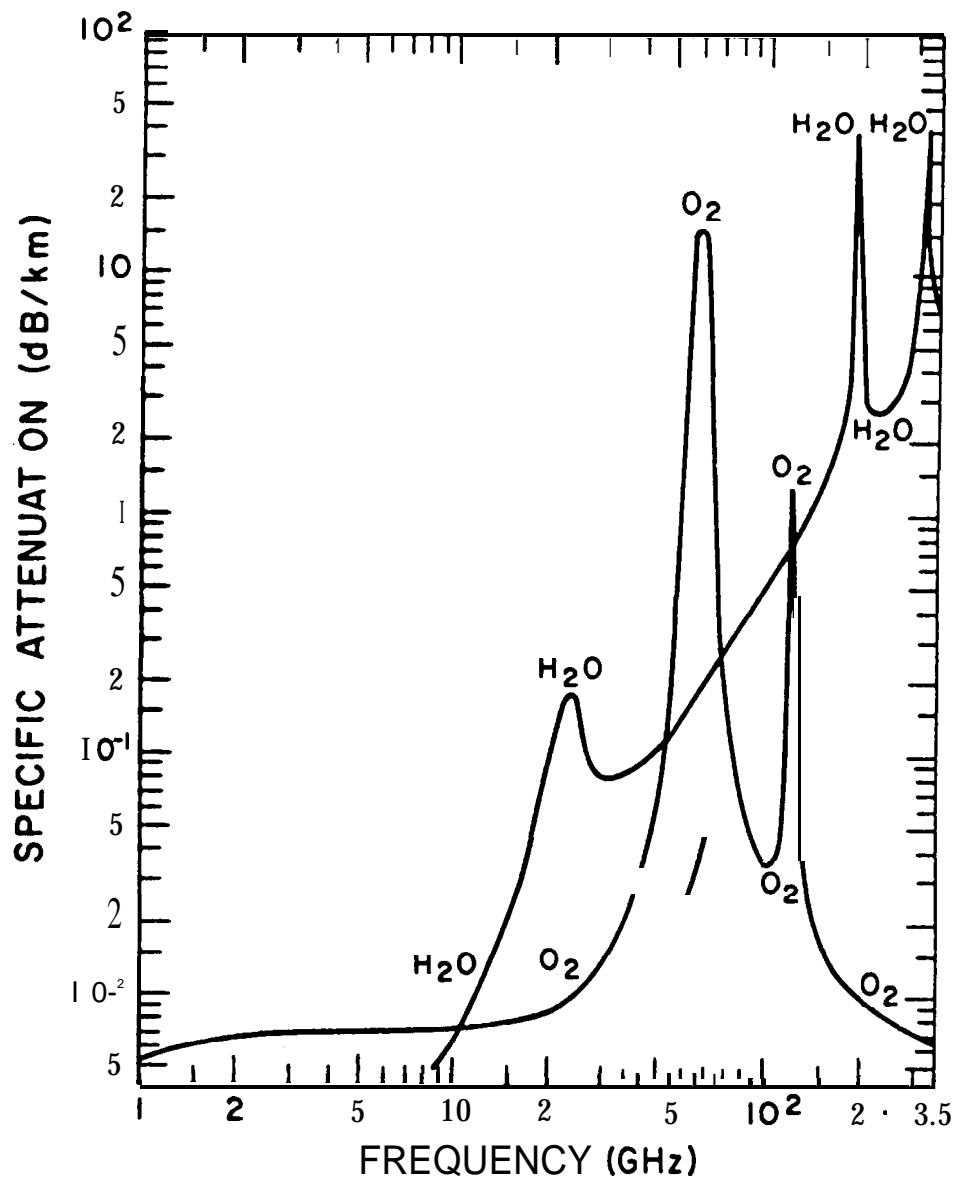


Figure 3.10. Attenuation constant for atmospheric gases for $p = 1013$ mb, $T = 15$ deg C, and $\rho = 7.5$ g/m³ (CCIR, 1986 b).

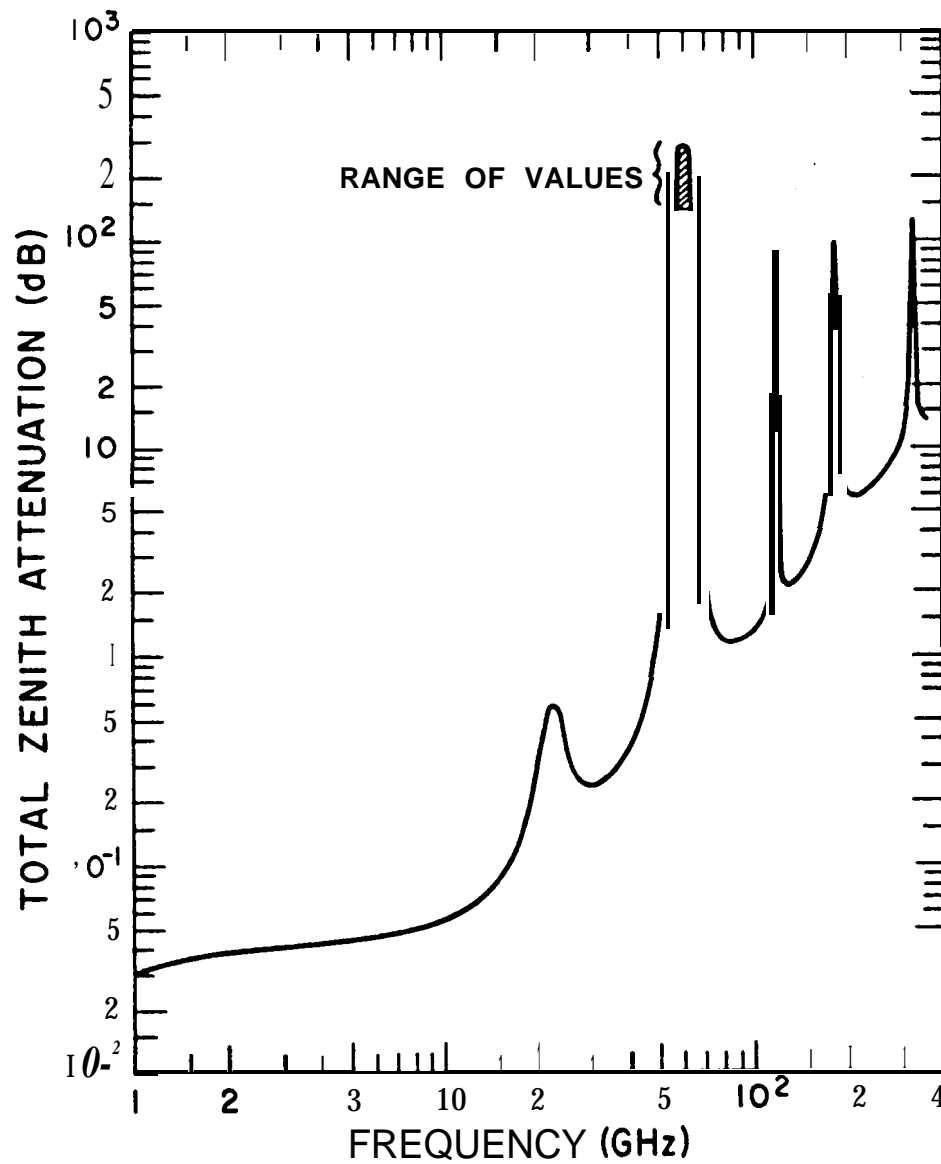


Figure 3.11. Total zenith attenuation at ground level for $p = 1013$ mb, $T = 20$ deg C, and $p_w = .5$ g/m³ (CCIR, 1986b).

$$a_w = \left[0.067 + \frac{2.4}{(f - 22.3)^2 + 6.6} + \frac{7.33}{(f - 183.5)^2 + 5} \right] f^2 \rho / 10^4 \quad (3.21)$$

with a_w in dB/km. The quantity ρ is water vapor density in g/m^3 .

An approximate expression for total attenuation A due to atmospheric gases for elevation angles $\theta > 10$ deg (CCIR, al 986b) is

$$A_a = \frac{8a_o + 2a_w}{\sin \theta} \quad \text{dB} \quad (3.22)$$

In CCIR (1986c) the relation given is

$$A_a = \frac{a_o \cdot h_o e^{-h_s/h_o} + \alpha_w h_w}{\sin \theta} \quad \text{dB} \quad (3.23)$$

where h_o is a characteristic distance for oxygen and is 6 km for $f < 57$ GHz and $h_w = 2.2 + 3/[(f - 22.3)^2 + 3]$ km for water vapor. The quantity h_s is the height in km of the earth station above sea level, and a_o and α_w are surface (sea level) attenuation constants for oxygen and water vapor.

3.7 TROPOSPHERIC EFFECTS ON RANGE, PHASE, AND DOPPLER FREQUENCY

Range to a target is commonly determined by radar techniques by assuming that electromagnetic waves propagate with the velocity c , about 2.9979×10^8 m/s. The velocity of c corresponds to an index of refraction of unity. In the troposphere, however, the index of refraction, n , is slightly greater than unity with the result that the velocity of an electromagnetic wave is slightly less than c . A range error then results if the velocity c is assumed. The slight error in range is unimportant in many applications but may be

important in other situations. In practice, when high accuracy in range is desired, an effort is made to estimate as accurately as possible the excess range delay (the amount by which the indicated range exceeds the true range) in order to correct for it (Flock, Slobin, and Smith, 1982).

Since 1983 the velocity of electromagnetic waves, c , has been taken to be the exact value of 299 792 458 m/s. The fractional uncertainty of c of $\pm 4 \times 10^{-9}$ that was previously stated is no longer applicable (Jennings, Evenson, and Knight, 1986). Along with specifying the above value of c , the meter was redefined to be consistent with c . Length and wavelength are now based on the same physical standard as time and frequency. When using time-of-propagation ranging techniques the time to distance conversion does not now increase uncertainty, as it tended to when the value of c was considered to have the fractional uncertainty stated above.

For the ionosphere (Sec. 2.3. 1), the range error AR can be determined by taking $\int (n - 1) dl$ along the path. For the troposphere, however, calculations are usually carried out by using the quantity $N = (n - 1) \times 10^6$. (In the ionospheric analysis, N stands for an entirely different quantity.) One may choose to treat dry air and water vapor separately. For dry air, making use of Eq. (3.3) for a zenith path,

$$A R_d = 10^{-6} \int N_d dl = 10^{-6} \int (77.6 \text{ pa}/T) dh \text{ m} \quad (3.24)$$

with AR_d the range delay due to dry air in m. The pressure p_d is in mb, h is height in m, and T is temperature in kelvins. Pressure in the troposphere tends to decrease 'exponentially as indicated by $p = p_0 e^{-h/H}$ [Eq. (1.18)], where H is the scale height kT/mg or RT/Mg , k is Boltzmann's constant, g is the acceleration of gravity (about 9.8 m/s^2 at the Earth's surface), R is the gas constant [$8.3143 \times 10^3 \text{ J}/(\text{K kg mol})$], M is the mass of a kg mol, and m is the mass of an individual molecule. ($M/m = 6.025 \times 10^{26}$, which corresponds to Avogadro's number but applies to a kg mol rather than a gram mol.) Using the form of H involving R with

$M = 28.9665$ from Table 3 of the U.S. Standard Atmosphere, 1976, treating T as if it were a constant, and employing the value of g utilized by Hopfield (1971) corresponding to the height at 500 mb at 45 deg latitude (namely, 9.7877 m/s^2).

$$\int_0^{\infty} p \, dh = \int_0^{\infty} p_0 e^{-h/H} \, dh = p_0 H = p_0 RT / (Mg) = p_0 T \cdot 29,326$$

Substituting the value of the integral into Eq. (3.24) and identifying P as P_{od} , the surface pressure of dry air

$$\Delta R_d = 2.2757 \times 10^{-3} p_{od} \quad (3.25)$$

with p_{od} in mb. If p_{od} is 1000 mb, for example, ΔR has the value of 2.28 m. The delay is directly proportional to the surface pressure of dry air and independent of the temperature profile. Hopfield (1971) has examined the applicability of this relation and has concluded that it allows determining the range error due to dry air on a zenith path to an accuracy of 0.2 percent or about 0.5 cm.

As H is a function of temperature and temperature varies with height, the exponential form $p \, dh \, e^{-h/H}$ with H a constant should only be assumed to apply over a limited height range. If account is taken of the variation of H with altitude, however, the integral of Eq. (3.24) can be represented as a summation of integrals over layers of limited thickness for which the values of T can be treated as constants. If this procedure is followed, T will cancel out of all the integrals and the same result will be obtained as shown by Eq. (3.25).

The delay caused by water vapor is considerably smaller than that for dry air, but total water vapor content along a path is variable and not predictable with high accuracy from the surface water vapor pressure or density. Therefore, water vapor is responsible for a larger error or uncertainty in range than is dry air. The expression for N_w , the contribution to refractivity of water vapor, is given by Eq. (3.5), but N_w can be expressed in terms of water vapor density ρ instead of water vapor pressure e , by using $e = \rho T / 216.5$ [Eq. (3.6)], and then takes the form

$$N_w = 0.3323 \rho + 1.731 \times 10^3 p / T \quad (3.26)$$

from which

$$AR_w = 10^{-6} \int N_w dl = 3.323 \times 10^{-7} \int \rho dl + 1.731 \times 10^{-3} \int (\rho/T) dl \quad (3.27)$$

Alternatively, the total excess range delay can be separated into ΔR_1 and ΔR_2 corresponding to the two terms of Eq. (3.3). This procedure has the practical advantages that it is easier to measure total pressure than the Pressure of dry air and that only one simple term is needed to determine each quantity whereas two dissimilar terms are involved in estimating AR_w . Following this procedure

$$AR_1 = 2.2757 \times 10^3 p_0 \quad m \quad (3.28)$$

where p. is now the total surface pressure and

$$\Delta R_2 = 1.731 \times 10^3 \int (p/T) dl \quad m \quad (3.29)$$

The value of the integral can be determined from radiosonde data if ρ and T vary cyl with height above the surface and not horizontally to a significant degree within the limits of the path.

Accumulation of sufficient data from radiosondes can provide a basis for a statistical description of the range error due to water vapor and for formulating models that may apply to particular locations. Radiosonde data are available from only certain locations, however, and it may be impractical to use radiosondes regularly and routinely for determining range errors due to water vapor. Aircraft instrumented with microwave refractometers can provide more accurate data on ρ and T.

Another approach is to employ microwave radiometry to estimate the value of AR_2 . This approach is based on the expression for brightness temperature T_b observed when a source at a temperature of T_s is viewed through an absorbing medium having a variable temperature T. T_b is given by (Waters, 1976, Wu, 1977)

$$T_b = T_s e^{-\tau_\infty} + \int_0^\infty T \alpha e^{-\tau} dl \quad (3.30)$$

with $\tau_{\infty} = \int_0^{\infty} \alpha dl$ and $\tau = \int \alpha dl$ where α is the variable attenuation constant (scattering neglected) at the frequency employed. The expression for T_b takes a simpler, and perhaps more familiar, form when T is constant or when an effective value T_i can be employed. In this case

$$T_b = T_s e^{-\tau} + T_i (1 - e^{-\tau}) \quad (3.31)$$

A problem with the radiometer method is that oxygen and perhaps liquid water contribute to α as well as water vapor. Use of a suitable pair of frequencies allows separating the effects of gaseous and liquid water to a reasonable degree, and the effect of oxygen can also be separated out (Staelin et al., 1977; Wu, 1977; Claflin, et al., 1978). Frequencies of 22.235 and 31.4 GHz have been used, 22.325 GHz being more sensitive to water vapor than liquid water by a factor 2.5 and 31.4 GHz being more sensitive to liquid water than vapor by about a factor of 2.

By using Eq. (3.30) for the two different frequencies, and with the terms involving T_s replaced by constants as T_s due to cosmic sources is small (about 2.7 K), a term $\int W(l) p/T dl$ is obtained where $W(l)$ can be made to have a nearly constant known value by a suitable choice of frequencies and other refinements described in the paper by Wu (1977). This approach to water-vapor radiometers has the appeal of being based on the physics of the problem and gives $\int \rho/T dl$ rather than the water-vapor content alone, $\int \rho dl$, which is what some other water-vapor radiometers were designed to provide.

A recent analysis of water-vapor radiometers for determining excess range delay has been prepared by Gary, Keihm, and Janssen (1985) who carried out simulation studies. Microwave brightness temperatures and excess range delay were calculated from radiosonde-based profiles of atmospheric parameters. A statistical retrieval technique was used to obtain retrieval coefficients relating path delay to observable (brightness temperature, surface-air temperature, pressure, and absolute humidity) for various combinations of frequencies. The relation used is

$$AR = C_0 + \sum C_i * O_i \quad (3.32)$$

where O_i represents the observable and C_o and C_i are computed by a least squares minimization technique involving the covariance matrices of the observable and path delay. Studies were included for which the surface observable were not included and for which only surface observable were used. Using three frequencies, 20.6, 22.2, and 31.4 GHz gives a small improvement over performance obtained by using only 20.6 and 31.4 GHz. Using surface values gives a modest improvement over results obtained by not using surface values. Surface values alone can be used but performance provided in this way is worse by a factor of 3 to 10 than that achievable by using radiometers. It is reported that it should be possible to correct path delay caused by water vapor with an accuracy better than 0.5 cm for zenith paths.

The exact value of ΔR_2 in a particular case depends on the value of the integral appearing in Eq. (3.29), but an indication of a representative magnitude of ΔR_2 can be obtained by assuming an exponential decrease of N_2 with a scale height H of 2 km. It is of interest that the value obtained in this way is the same as if N_2 were constant up to the height H and zero beyond. Assuming a vapor density ρ of 7.5 g/m^3 at the surface and a temperature of 280 K, the corresponding values of e and N_2 at the surface are 9.70 mb and 46.15 respectively. Then for a vertical path

$$\begin{aligned} \Delta R_2 &= 10^{-6} \int_0^{\infty} 46.15 e^{-h/2000} dh = 10^{-6} (46.15)(2000) - \\ &= 0.0923 \text{ m} = 9.23 \text{ cm}. \end{aligned}$$

An extreme value of ΔR_2 , corresponding to the highest accepted weather-observatory values of e and ρ of 53.2 mb and 37.5 g/m^3 at the temperature of 34 deg C and assuming an exponential decrease of N_2 with a scale height of 2 km, is 42.1 cm, for a vertical path.

Once a ΔR value is known, a corresponding phase angle ϕ can be determined by use of

$$\Delta\phi = \Delta R \beta = \Delta R (2\pi/\lambda) \quad \text{rad} \quad (3.33)$$

where β is the phase constant and is equal to $2\pi/\lambda$. The doppler

frequency error f_D associated with the range and phase errors is given by

$$f_D = \frac{1}{2\pi} \frac{A(\#)}{\Delta t} \quad (3.34)$$

where the rate of change of phase with time is involved. Thus f_D involves the rate of change of refractivity along the path. The value given by Eq. (3.34) may also depend in practice to some extent on the interval of time Δt used to measure $\Delta\phi$.

For paths at an elevation angle θ of about 10 deg or greater, the range delay equals the vertical or zenith value divided by $\sin \theta$. That is,

$$\Delta R(\theta) = AR/\sin \theta \quad (3.35)$$

Table 3.3 shows values of $AR(\theta)$ or range error for elevation angles of 0, 5, and 50 deg, based on the 1966 Standard Atmosphere for 45 deg N latitude in July and including an assumed humidity-profile model. These values represent total delay due to both the dry component of air and water vapor. Note the large values of range error for 0 and 5 deg.

The widely used constants provided by Smith and Weintraub (1953) have been employed for calculating refractivity in this chapter. When extreme precision is important, reference can be made to values provided by Thayer (1974).

The excess range delay due to the troposphere (and stratosphere) has also been treated by Saastamoinen (1972). He developed the following expression, which takes account of dry air, water vapor, and atmospheric refraction.

$$AR = 2.277 \times 10^{-3} \text{ sec } z [p + (1255/T + 0.05)e^{-1.16 \tan 2z}] \quad (3.36)$$

The quantity z is the zenith angle and the other quantities have the same meaning as previously in this chapter.

The number 2.277×10^{-3} differs slightly from 2.2757×10^{-3} of Eq. (3.28) because Saastamoinen used a 1963 expression for refractivity by Essen and Frome rather than the expression used elsewhere in this chapter by Smith and Weintraub (1953). Also he

used 9.784 m/s^2 for g rather than 9.7877 m/s^2 as in the derivation of Eq.(3.28). He included an expression for g as a function of latitude ϕ and station height H above sea level, namely

$$g = 9.784 (1 - 0.0026 \cos 2\phi - 0.00028 H) \text{ m/s}^2 \quad (3.37)$$

However he asserted that because of limitations of the ranging process it was sufficient and accurate to use 9.784 m/s^2 for g for all latitudes and station heights. For a pressure of 1013 mb and a zenith path the factor 2.277×10^{-3} of Eq.(3.36) gives a value of 2.3066 m for excess range delay, compared with 2.3053 m for ΔR_1 when Eq.(3.28) is utilized.

The quantity $2.277 \times 10^{-3} [1255/T + 0.05] e$ of Eq.(3.36) is suitable for obtaining illustrative or approximate values of the additional excess range delay due to water vapor. For a temperature T of 280 K and water vapor' pressure e of 9.70 mb, this quantity gives an excess range delay of 10.01 cm. The assumption of a particular exponential profile for illustrating the delay due to water vapor earlier in this section gave a delay of 9.23 cm for the same values of T and e . Part of the difference is due to the fact that in the treatment of this chapter no term like the coefficient 0.05 of Eq. (3.28) is recognized because if total pressure is used for ΔR_1 of Eq. (3.28) the remaining delay due to water vapor ΔR_2 is given by only a single term. But if 0.05 is eliminated from Eq. (3.36) the delay of 10.01 cm is reduced only to 9.90 cm.

3.8 EXCESS RANGE DELAY IN LASER RANGING

This handbook does not attempt to treat optical propagation, but, because it is of interest to persons concerned with tropospheric excess range delay at microwave frequencies to know what the corresponding situation is at optical frequencies, we include this mention of laser ranging. The' clear air is dispersive at optical frequencies, and the group refractivity $N_g = (n_g - 1) \times 10^6$ affects excess range delay. The following expression for N_g is given by Abshire and Gardner (1985) and credited to Marini and Murray.

$$N_g = 80.343 f(\lambda) p/T - 11.3 e/T \quad (3.38)$$

The quantities p , T , and e have the same meaning and are in the same units (mb for p and e , K for T) as in the previous expressions for radio frequencies. The term $f(\lambda)$ describes the variation of N_g with wavelength and has the form of

$$f(\lambda) = 0.9650 + 0.0164/\lambda^2 + 0.000228/\lambda^4 \quad (3.39)$$

with λ in μm . The dispersive nature of the atmosphere allows the possibility of two-color (two-frequency) laser ranging such that

$$\Delta R_1 = \gamma (R_2 - R_1) \quad (3.40)$$

with $\gamma \approx \frac{f(\lambda_2) - f(\lambda_1)}{f(\lambda_2 - \lambda_1)}$

where the subscripts 1 and 2 refer to the two frequencies, R_2 and R_1 are the measured ranges at the two frequencies, and ΔR_1 is the excess range delay at frequency one. Note that the procedure is similar to that described for ionospheric propagation (Sec. 2.3.1), for which the use of two frequencies allows solving for the TEC and the time and range delays at the two individual frequencies.

REFERENCES

- Abshire, J. B. and C. S. Gardner, "Atmospheric refractivity corrections in satellite laser ranging," IEEE Trans. Geosci. Remote Sensing, vol. GE-23, pp. 414-425, July 1985.
- Bean, B. R. and E. J. Dutton, Radio Meteorology. Washington, DC: Supt. of Documents, U.S. Government Printing Office, 1966.
- Bean, B. R., J. D. Horn, and O. M. Ozanich, Climatic Charts and Data of the Radio Refractive Index for the United States and the World, National Bureau of Standards Monograph 22. Washington, DC: Supt. of Documents, U.S. Government Printing Office, Nov. 25, 1960.
- Bean, B. R., B. A. Cahoon, C. A. Samson, and G. D. Thayer, A World Atlas of Atmospheric Radio Refractivity, ESSA Monograph 1. Washington, DC: Supt. of Documents, U.S. Government Printing Office, 1964.
- CCIR, "Radiometeorological data," Report 563-3, Vol. V, Propagation in Non-ionized Media, Recommendations and Reports of the CCIR, 1986. Geneva: Int. Telecomm. Union, 1986a.
- CCIR, "Attenuation by atmospheric gases," Report 719-2, Vol. V, Propagation in Non-ionized Media, Recommendations and Reports of the CCIR, 1986. Geneva: Int. Telecomm. Union, 1986b.
- CCIR, "Propagation data and prediction methods required for Earth-space telecommunication systems," Report 64-3, Vol. V, Propagation in Non-ionized Media, Recommendations and Reports of the CCIR, 1986. Geneva: Int. Telecomm. Union, 1986c.
- Clafin, E. S., S. C. Wu, and G. M. Resch, "Microwave radiometer measurement of water vapor path delay: data reduction techniques," in DSN Progress Report 42-48, Jet Propulsion Laboratory, Pasadena, CA, Sept.-Oct. 1978.
- Crane, R. K., "Refraction effects in the neutral atmosphere," in Methods of Experimental Physics, Vol. 12, Astrophysics, Part B: Radio Telescopes (M. L. Meeks, ed.), pp. 1/6-200, New York: Academic Press, 1976.
- Dugherly, H. T. and B. A. Hart, Anomalous Propagation and Interference Fields, Report 76-107, Department of Commerce, 1976.

- Dougherty, H. T. and B. A. Hart, "Recent progress in duct propagation predictions," *IEEE Trans. Antennas Propagat.*, vol. AP-27, pp. 542-548, July 1979.
- Flock, W. Lo, Electromagnetics and the Environment: Remote Sensing and Telecommunications. Englewood Cliffs, NJ: Prentice-Hall, 1979.
- Flock, W. L., S. D. Slobin, and E. K. Smith, "Propagation effects on radio range and noise in earth-space telecommunications," *Radio Sci.*, vol. 17, pp. 1411-1424, Nov. -Dec. 1982.
- Gary, B. L., S. J. Keihm, and M. A. Janssen, "Optimum strategies and performance for the remote sensing of path delay using ground-based microwave radiometer," *IEEE Trans. Geosci. Remote Sensing*, vol. GE-23, pp. 479-484, July 1985.
- GTE Lenkurt, Engineering Considerations for Microwave Communication Systems. San Carlos, CA: GTE Lenkurt, Inc., 1972.
- Hall, M. P. M., Effects of the Troposphere on Radio Communications. Stevenage, UK and New York: Peter Peregrinus (on behalf of IEE). 1979.
- Hautefeuille, M. A. et al., "Duct fading - is Senegal an isolated case?," *Telecomm. Jour.*, vol. 47, pp. 517-525, 1980.
- Hopfield, H. S., "Tropospheric effect on electromagnetically measured range: prediction from surface weather data," *Radio Sci.*, vol. 6, pp. 357-367, March 1971.
- Jennings, D. A., K. M. Evenson, and D. J. E. Knight, "Optical frequency measurements," *Pmt. IEEE*, vol. 74, pp. 168-179, Jan. 1986.
- Liebe, H. J., "An updated model for millimeter wave propagation in moist air," *Radio Sci.*, vol. 20, pp. 1069-1089, Sept.-Ott. 1985.
- List, R. J., Smithsonian Meteorological Tables, Sixth Revised Ed., 5th Reprint, Washington, DC: Smithsonian Institution, 1984.
- Resch, G. M., "Water vapor - the wet blanket of microwave interferometry," in Atmospheric Water Vapor (A. Deepak, T. D. Wilkerson, L. H. Ruhnke, eds.), pp. 265-282. New York: Academic Press, 1980.
- Saastomoinen, J., "Atmospheric correction for the troposphere and stratosphere in radio ranging of satellites," in Geophys. Monogr. Ser., vol. 15, The Use of Artificial Satellites for Geodesy, ed. by S. W. Henriksen et al., pp. 241-251, AGU, Washington, DC.

- Smith, E.K. and S. Weintraub, "The constants in the equation for atmospheric refractive index at radio frequencies," Proc. IRE, vol.41, pp. 1035-1037, August 1953.
- Smith, E. K., "Centimeter and millimeter wave attenuation and brightness temperature due to atmospheric oxygen and water vapor," Radio Sci., vol.1 7, pp. 4455-1464. Nov.-Dec.1 982,
- Staelin, D. H. et al., "Microwave spectroscopic imagery of the earth," Science, vol. 197, pp. 991-993, Sept. 2, 1977.
- Strickland, J. I., R. I. Olsen, and H. L. Werstivk, "Measurements of low angle fading in the Canadian Arctic," Ann. Telecomm., VOL 32, pp. 530-535, 1977.
- Thayer, G. D., "An improved equation for the radio refractive index of air," Radio Sci., vol. 9, pp . 803-807, Oct. 1974.
- Theobald, D. M. and R. Kaul, "Prediction of signal fluctuations and low angle fading on earth-space paths," in Prediction of Millimeter Wave Propagation Effects on Earth-Space Paths (10-100 GHz), ORI, Inc., Section IV, Greenbelt, MD: NASA Goddard Space Flight Center, 1978.
- Thompson, M. C., L. E. Wood, H. B. Janes, and D. Smith, "Phase and amplitude scintillations in the 10 to 40 GHz band," IEEE Trans. Antennas Propagat., vol. AP-23, pp. 792-'797, Nov. 1975.
- U. S. Standard Atmosphere, 1976 sponsored by NOAA, NASA, USAF. Washington, DC: Supt. of Documents, U.S. Government Printing Office, 1976.
- Van Vleck, J. H., "Theory of absorption by uncondensed gases," in Propagation of Short Radio Waves, Vol. 13, Radiation Lab. Series (D. E. Kerr, ed.), pp. 649-664. New York: McGraw-Hill, 1951.
- Waters, J. W., "Absorption and emission by atmospheric gases," in Methods of Experimental Physics, Vol. 12, Astrophysics, Part B: Radio Telescopes (M. L. Meeks, cd.), pp. 142-176. New York: Academic Press, 1976.
- Weisbrod, S. and L. J. Anderson, "Simple methods for computing tropospheric and ionospheric refractive effects on radio waves," Proc. RE, vol. 47, pp. 1770-1777, Oct. 1959.
- Wu, so c., "Frequency selection and calibration of a water vapor radiometer," in DSN Progress Report 42-43, Jet Propulsion Laboratory, Pasadena, CA, pp. 67-81, Nov. -Dec., 1977.